# Supporting Information for "Eddy impacts on the marine biogeochemistry of the California Current System"

Pierre Damien[1], Daniele Bianchi[1], Fayçal Kessouri[2], James C. McWilliams[1]

[1]University of California, Los Angeles, CA

[2]Southern California Coastal Water Research Project, Costa Mesa, CA

## Contents of this file

1. Texts T1 to T3

2. Figures S1 to S6

## Introduction

This file contains information on the computation of the triple eddy decomposition (T1), the mathematical formulation of the nutrient uptake in the biogeochemical model used in the study (T2), and additional figures complementing the results section of the main paper (T3).

## 1. Technical details for the triple decomposition

The proposed decomposition method relies on two filters that aim to separate the mean field associated with regional and seasonal variations from the mesoscale and submesoscale fields associated with turbulence in these dynamical regimes. This decomposition is made delicate by the absence of clear boundaries between these regimes. In fact, a certain degree of overlapping exists making the choice of the filters partly subjective. Practically, we tested several space, time, and combined space-time filters, and finally opt for the combination of space and time box-averaging filters defined as follows :

- $\overline{\tau}$ : 3 months and 15 km center averaging,
- $\widetilde{\tau}$ : 3 days and 5 km center averaging.

Although not providing an excellent precision in the selected cut-off scale, this method is widely used in ocean dynamics to decompose mean and eddy flows. Figures S1 and S2 expose the performance of this decomposition on temperature $T$ and vertical velocity $w$ fields at 25m in the CCS. As expected, the upwelling signal, characterized by cold water along the coast, is largely contained in $\overline{T}$. $T'$ exhibits the large positive and negative anomalies with moderate gradients expected at mesoscale while sharp filamentary and frontal anomalies characterized $T''$ at submesoscales. Submesoscale is also associated with the large majority of vertical motions, as ageostrophic current start to be significant at submesoscale. Figure S3 presents the mesoscale and submesoscale eddy variance of several tracers and momentum at 25m depth. They both reach large magnitude compared to their low-frequency state. Except for vertical velocities, variance at mesoscale is significantly larger than at submesoscale.

The major downside of the spatial filtering method is the question of the boundary. Close to the coast, it induces a "shadow zone" of half the filter width. We excluded this region for the analysis and leave a dedicated assessment to future studies. A way to overcome this issue could rely on the use of degraded filters or exclusively time-based (space or frequency) filters along the coast.

The decomposition of any biogeochemical equation requires the online computation of daily averages of the equation trend terms and of the tracer fields. The online averaging of the rates and fluxes allows to capture a signal frequency as high as the model can provide, i.e. corresponding to the temporal and spatial resolution of the model. Then, mean terms are computed offline applying

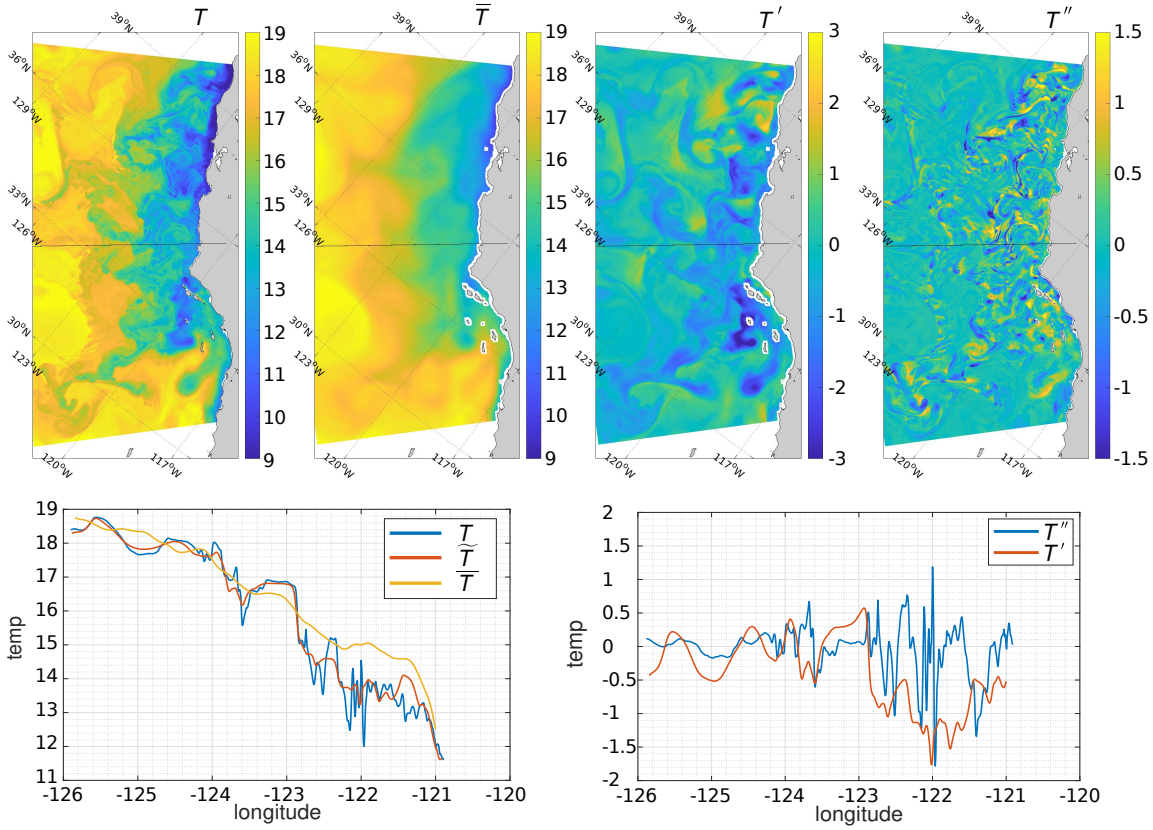


**Figure S1.** Triple decomposition applied to a temperature field at 25 m depth: (Upper panels from left to right) temperature snapshot and its decomposition into mean, mesoscale, and submesoscale components; (lower panels) cross-sections of the filter products at 35.4N (black line on the upper panels)

the flux formulation on filtered tracer fields. The eddy terms are computed by differences :

$$J^{mean} = J(\overline{X_i}) \tag{1}$$

$$J^{meso} = J(\widetilde{X_i}) - J(\overline{X_i}) \tag{2}$$

$$J^{subm} = J(X_i) - J(\widetilde{X_i}) \tag{3}$$

In a Reynolds decomposition, the eddy terms arise from the eddy-scale correlations between momentum and biogeochemical tracers. Since the chosen filters are not strictly orthogonal, the

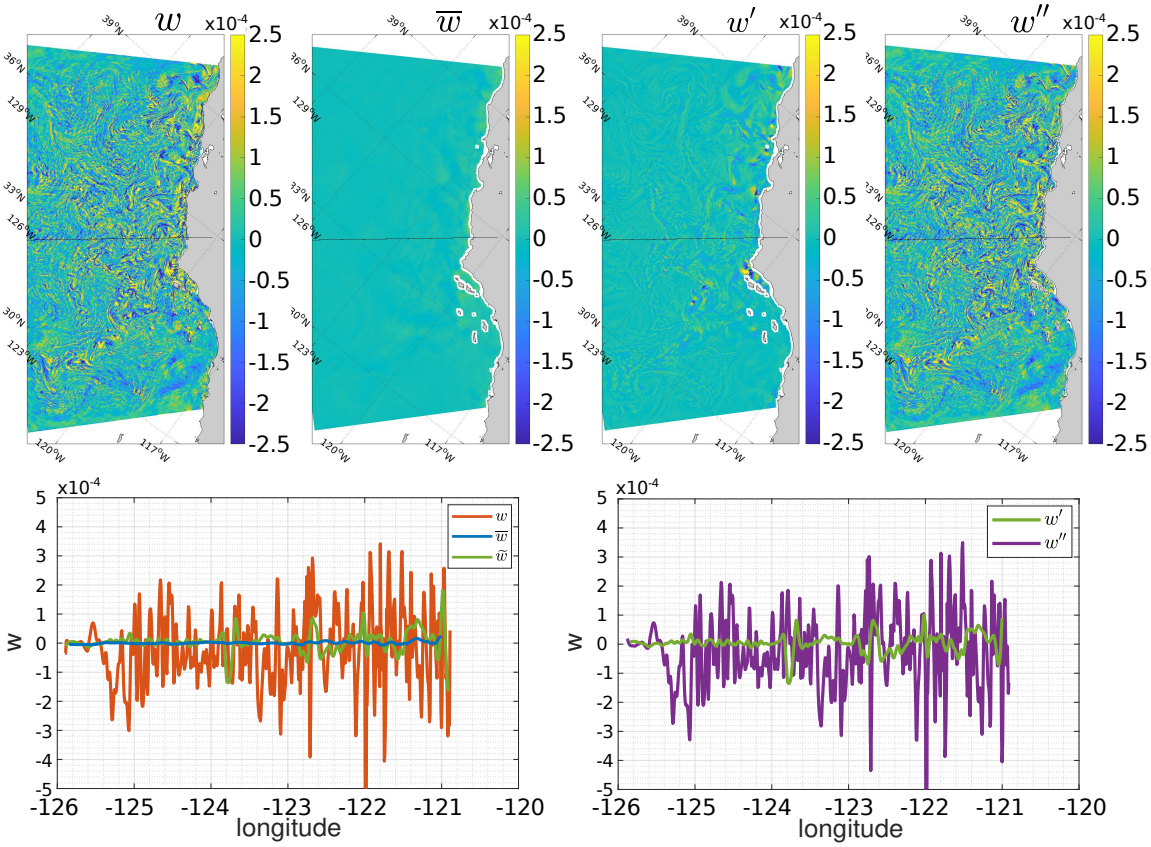


**Figure S2.** Same as Fig. S1 except for vertical velocity.

necessary condition $\overline{\overline{X_i}} = \overline{X_i}$ for the cross-terms to vanish, is not necessarily satisfied. As a results, the Reynolds decomposition does not strictly apply here. However, the chosen method has the major advantage to retrieve an eddy turbulent flux by differences between total and mean flux. The drawback is that it might also account for non-negligible cross terms arising from the correlation between the mean and eddy components of momentum and tracers.

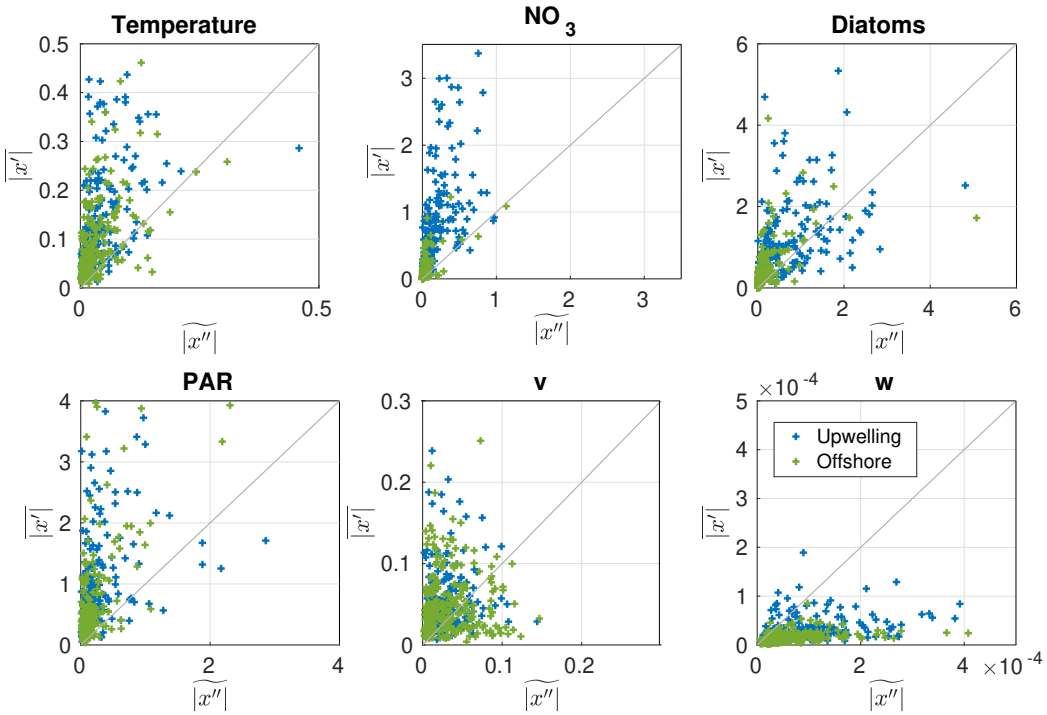


**Figure S3.** Mesoscale and submesoscale eddy variance of temperature, nitrate, phytoplankton, radiation, horizontal and vertical velocity at 25m depth. The mesoscale and submesoscale standard deviations are defined as respectively $\overline{|x'|} = \sqrt{\sum_{i=1}^{\overline{\tau}} (\widetilde{x} - \overline{x})}/\overline{\tau}$ and $\widetilde{|x''|} = \sqrt{\sum_{i=1}^{\widetilde{\tau}} (x - \widetilde{x})}/\widetilde{\tau}$. Except for vertical velocities, variability at mesoscale tends to be larger than at submesoscale. Since the eddy transport and reaction grow on the variability of tracers and momentum at eddy scales, the variability in determined frequencies range gives an indication on the magnitude of the eddy transport and reactions.

Assuming $\overline{\overline{X_i}} = \overline{X_i}$ and $\widetilde{\widetilde{X_i}} = \widetilde{X_i}$, $J^{meso}$ and $J^{subm}$ relate to the eddy $X_i$ as follows:

$$
\begin{aligned}
\partial_t \widetilde{x} &= \widetilde{J}(x_{k=1,\dots,n}) \\
&= J(\widetilde{x}_{k=1,\dots,n}) + \widetilde{J}(x''_{k=1,\dots,n}) \\
\partial_t \overline{\widetilde{x}} &= \overline{J}(\widetilde{x}_{k=1,\dots,n}) + \overline{\widetilde{J}}(x''_{k=1,\dots,n}) \\
&= J(\overline{\widetilde{x}}_{k=1,\dots,n}) + \overline{J}(\widetilde{x}'_{k=1,\dots,n}) + \overline{\widetilde{J}}(x''_{k=1,\dots,n})
\end{aligned}
\tag{4}
$$

$J(x_{k=1,...,n})$ stands for physical and biogeochemical fluxes. Since $\tau_{\overline{filt}} >> \tau_{\widetilde{filt}}$ , we assume $\overline{\overline{x}} \approx \overline{x}$, implying :

$$\partial_t \overline{x} = \underbrace{J(\overline{x}_{k=1,...,n})}_{\overline{J^{mean}}} + \underbrace{\overline{J(\widetilde{x}'_{k=1,...,n})}}_{\overline{J^{meso}}} + \underbrace{\overline{J(x''_{k=1,...,n})}}_{\overline{J^{subm}}} \quad (5)$$

## 2. Eddy uptake

In BEC, the mathematical formulation of the nitrate biological uptake $J^{Uptk}$ expressed as :

$$J^{Uptk} = -Q_{N:C} \frac{V_{NO_3}}{V_{NO_3} + V_{NH_4}} J_C^{photo} \quad (6)$$

$$V_{NO_3} = \frac{NO_3/k_{NO_3}}{1 + NO_3/k_{NO_3} + NH_4/k_{NH_4}} \quad (7)$$

$$V_{NH_4} = \frac{NH_4/k_{NH_4}}{1 + NO_3/k_{NO_3} + NH_4/k_{NH_4}} \quad (8)$$

$$V_{Fe} = \frac{Fe}{Fe + k_{Fe}} \quad (9)$$

$$V_{PO_4} = \frac{PO_4}{PO_4 + k_{PO_4}} \quad (10)$$

$$V_{SiO_2} = \frac{SiO_2}{SiO_2 + k_{SiO_2}} \quad (11)$$

$$J_C^{photo} = \mathrm{PC}_{\mathrm{ref}}\, f_{nut}\, T_{func} \left(1 - e^{-\frac{\alpha_{chl}\, Q_{Chl:C}\, PAR}{\mathrm{PC}_{\mathrm{ref}}\, f_{nut}\, T_{func}}}\right) C_{phyto} \quad (12)$$

$$f_{nut} = \min(V_{NO_3} + V_{NH_4}, V_{Fe}, V_{SiO_2}, V_{PO_4}) \quad (13)$$

$$T_{func} = 2^{0.1*T-3} \quad (14)$$

with $T_{func}$ a temperature dependency, $Q_{N:C}$ the constant stochiometric ratio of nitrogen over carbon, $\mathrm{PC}_{\mathrm{ref}}$ the constant maximum phytoplankton C-specific growth rate at given temperature set to 3.0 $\mathrm{d}^{-1}$, $f_{nut}$ the nutrient limitation function, $Q_{Chl:C}$ the variable ratio of chlorophyll over

carbon in phytoplankton, and $\alpha_{chl}$ the chlorophyll-specific initial slope of P vs. I curve. $k_{NO_3}$, $k_{NH_4}$, $k_{Fe}$, $k_{PO_4}$, $k_{SiO_2}$ are the half saturation constant for nutrient uptake.

This formulation beholds multiple sources of non-linearities that allows an eddy rectification to emerge. The most evident ones are the covariance between nutrient ($N$) and phytoplankton ($P$) concentrations, the exponential temperature ($T$) dependency that also co-varies with nutrient and phytoplankton concentrations, and the exponential growth with light ($L$). These multiple eddy correlations ($N-P-T-L$) coupled to functional dependencies contribute to the magnitude of the eddy uptake and define its sign. However, we found that, averaged over the high frequency fluctuation period, the eddy uptake is largely negative (Fig. **??** and **??**)

Assuming high frequency fluctuations of small amplitudes, we can approximate the rectified effect by a Taylor series expansion :

$$\overline{J^{eddy}} \approx \sum_i \frac{\partial J}{\partial X_i}\bigg|_{\overline{X_i},\overline{X_j},\ldots} \overline{X_i'} + \frac{1}{2}\sum_{i,j} \frac{\partial^2 J}{\partial X_i \partial X_j}\bigg|_{\overline{X_i},\overline{X_j},\ldots} \overline{X_i' X_j'} \tag{15}$$

Because the fluctuations have zero average, the linear terms disappear and the sign and amplitude of the eddy rectification depend on the curvature of the functional dependencies and the eddy correlation term. A comparison of the different contribution for the uptake rectification (Fig. S4) evidences that $N'N'$ and $N'P'$ are dominant at mesoscale and submesoscale. This is largely due to the larger magnitudes of the second uptake derivatives that modulate the quadratic terms. The negative sign of the uptake rectification mainly arises from the product of $N'^2$, positive by definition, and the Michaelis-Menten nutrient growth dependencies with negative curvature. This rectification is increased at subsurface by the $N'P'$ where nutrients and phytplankton are negatively correlated, and is partly compensated at surface by the covariance of the same vari-

ables. The other terms are overall less significant with the exception of the highly productive coast.

## 3. Additional figures completing the mean-eddy decomposition

This section includes additional figures that complement the result section and support the discussion.

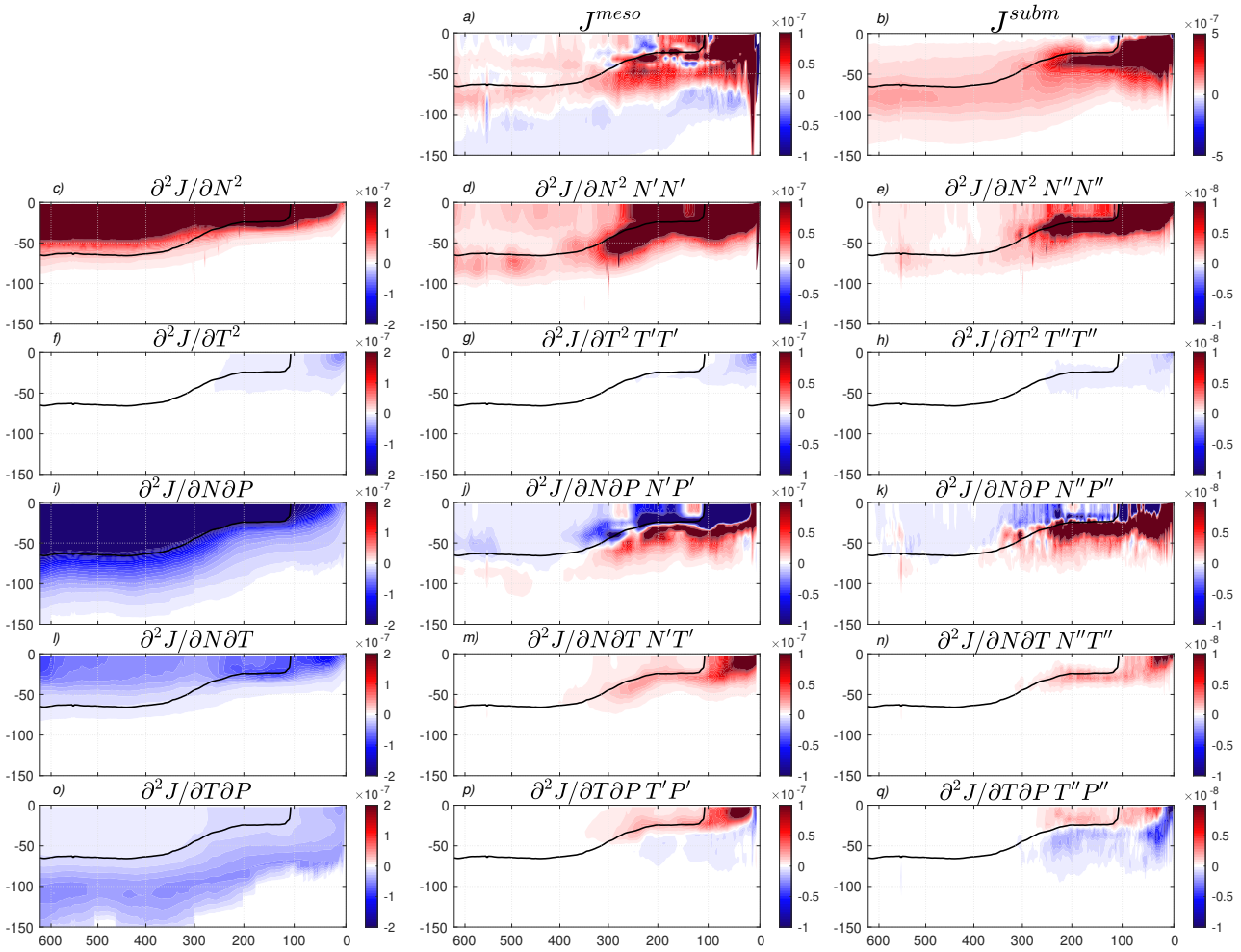


**Figure S4.** Cross sections, as a function of off-coast distance and depth, of the annual mean (a) mesoscale and (e) submesoscale eddy uptake, (c,f,i,l,o) the second derivative terms that modulate the (d,e) nutrient and (g,h) temperature autocorrelation, (j,k) nutrient-phytoplankton eddy covariance, (m,n) nutrient-temperature eddy covariance, and (p,q) temperature-biomass eddy covariance at mesoscale and submesoscale. Units for uptake rates are mmol $m^{-3}$ $s^{-1}$. The thick black contour represents the nutricline defines as a nitrate concentration of 1 mmol.$m^{-3}$. Note that the computation of the submesoscale eddy covariance was performed on daily averaged variables for numerical storage reason. Consequently, this approach leads to a significant underestimation of submesoscale variability, resulting in an underestimation of the magnitude of the submesoscale terms. Due to numerical storage limitation, we can only accurately diagnose the eddy reactions for the mesoscale. However, we remark that a partial diagnosis of submesoscale reactions based on daily average variables lead to similar result than the mesoscale diagnosis, but with different amplitude.

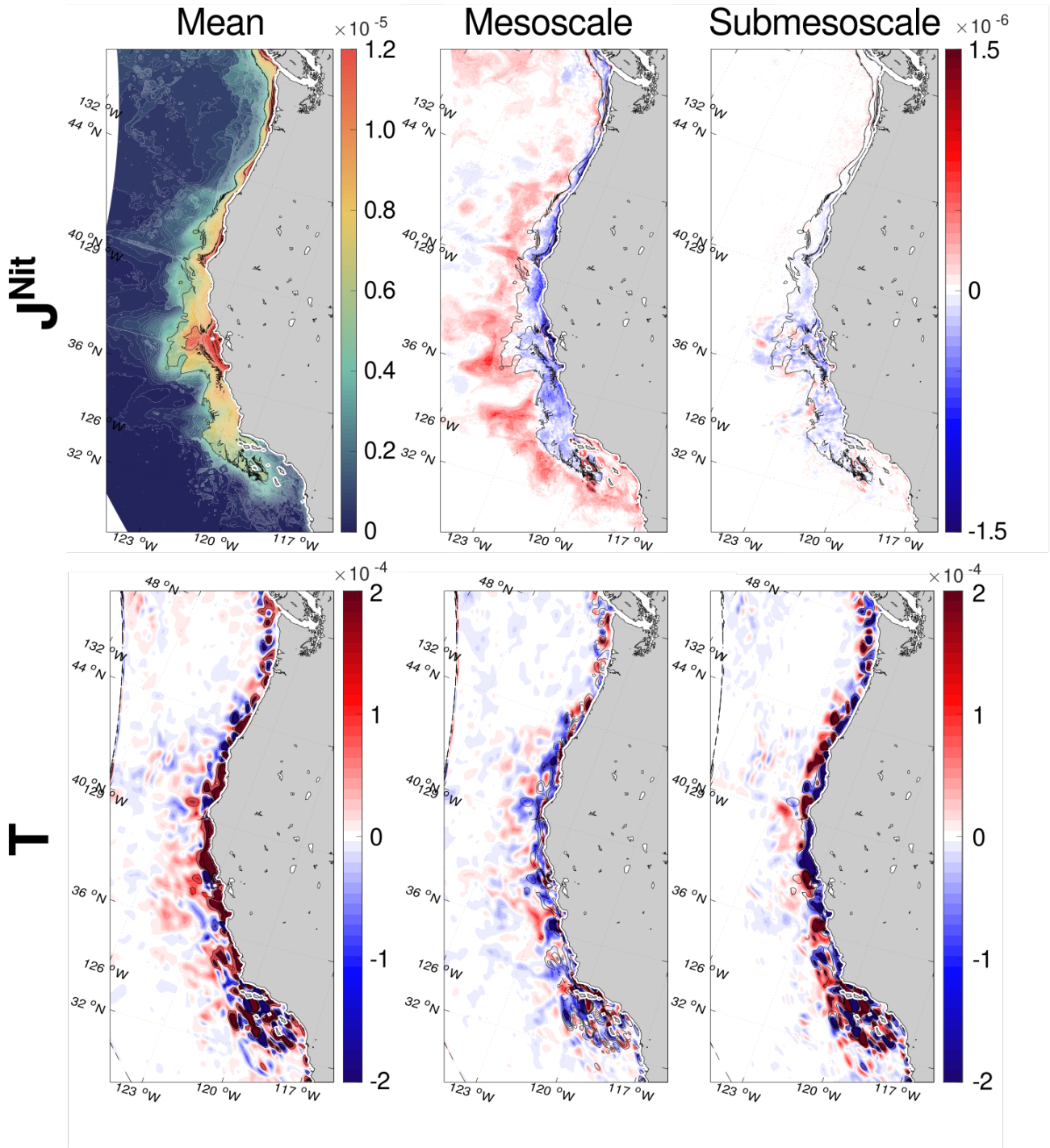


**Figure S5.** Triple decomposition of yearly averaged (upper panels) nitrification, and (lower panels) $NO_3^-$ transport divergence integrated over the euphotic layer: (from left to right) mean, mesoscale, and submesoscale. Units are mmol $m^{-2}$ $s^{-1}$

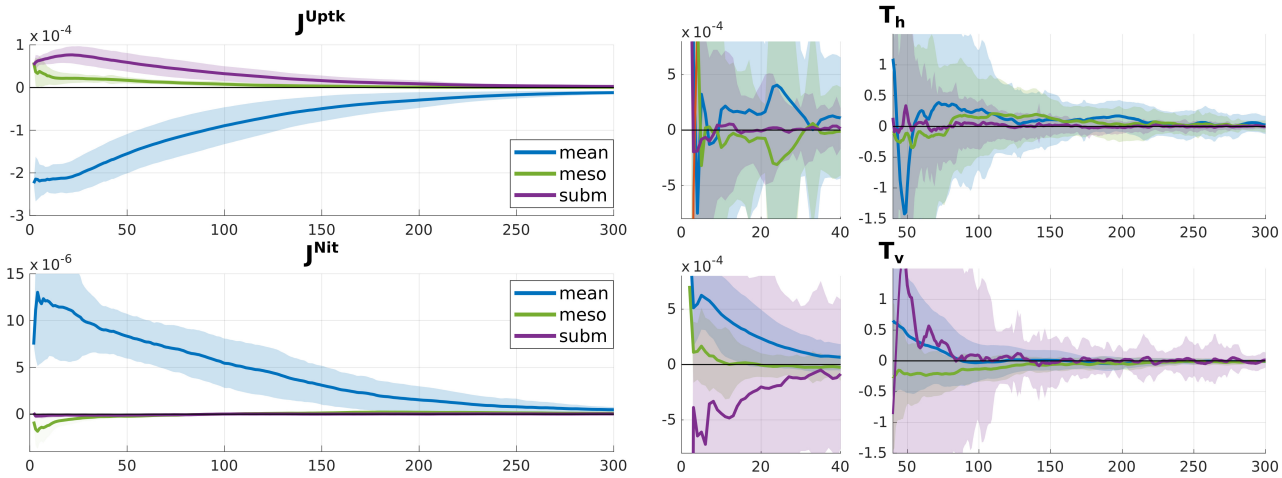


**Figure S6.** Cross-sections of the (blue) mean, (green) mesoscale, and (purple) submesoscale terms of the $NO_3^-$ balance averaged over a full seasonal cycle and integrated meridionally over the upwelling region, from Point Concepcion to Cape Blanco. The light shaded area is the meridonal standard deviation. The cross-sections of flux divergence is divided into coast and offshore with different y-axis scales. Units are mmol $m^{-2}$ $s^{-1}$.